

# BALLOON VARIANT OF SINGLE SPOKE RESONATOR

Z. Yao<sup>#</sup>, R.E. Laxdal, V. Zvyagintsev, TRIUMF, Vancouver, B.C., Canada

## Abstract

Spoke resonators have been widely proposed and optimized for various applications. Good performance has been demonstrated by many cold tests. Accompanying the great progress, the adverse impact of strong multipacting (MP) is also noted by recent test reports, consistent with modern 3D simulations. This paper will discuss MP behaviors in the single spoke resonator. In particular a phenomenological theory is developed to highlight the details of the geometry that affect MP. The analysis leads to an optimized geometry of a single spoke resonator defined here as the ‘balloon geometry’.

## INTRODUCTION

Spoke resonators have been widely proposed as the accelerating cavity type of the low-medium energy section in several proton and ion LINAC projects like PIP-II [1], ESS [2], MYRRHA [3], CAD5 [4] and RAON [5]. Recently, the application of the spoke resonators is extended to electron LINACs like the compact ERL-LCS [6]. The additional focus on the spoke resonator has prompted further optimized geometries with low Epeak/Eacc values around 4 and Bpeak/Eacc values around 6 mT/(MV/m) [5, 7-12]. With these optimizations higher accelerating gradients are predicted to be achieved. To date an accelerating gradient of 22MV/m was demonstrated by Fermilab [13] in a low  $\beta$  resonator.

Despite the successes spoke resonators have a reputation as being sensitive to MP. Strong MPs during cavity cold tests were reported by ODU[14], IHEP[12], and Fermilab[15]. As spoke cavities are pushed to higher accelerating gradients and quality factors a deeper understanding of MP issues is required to avoid reduced performance during operation. MP is dependent on secondary electron resonance and the surface secondary electron yield (SEY) properties of niobium. In this paper we analyze the MP phenomenon and demonstrate the relationships between the local electro-magnetic (EM) field distributions and MP. A phenomenological theory is proposed that is then used to develop an optimized geometry for a single spoke resonator with regards to MP suppression.

## CHARACTERISTICS OF MULTIPACTING

The common features of MP in the single spoke resonator are studied with CST [16]. For the generic study, we consider the simple spoke model shown in Fig. 1. The model is not optimized for any application or geometry  $\beta$  range. The cavity voltage excluding the transient time factor is used to define the RF field level. The resonance frequency is in the range 325...350MHz, a common frequency range for spoke resonator applications.

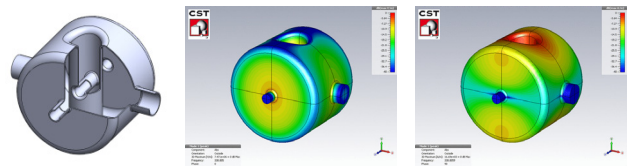


Figure 1: A simplified single spoke resonator model for a generic MP study with surface electric and magnetic field distributions.

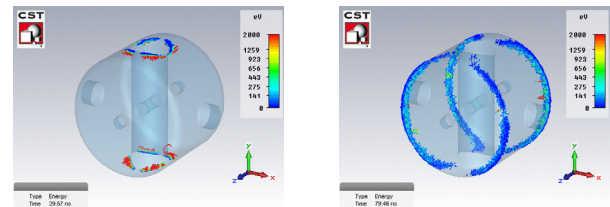


Figure 2: Typical secondary electron trajectories and resonance position of 1st order (left) and higher order (right) MPs in single spoke resonators.

Particle trajectories of various orders of MP are shown in Fig. 2. The secondary electron number will grow exponentially if MP happens in a stable resonance path. The exponential fit parameter is defined as growth rate of that certain order MP. The impact-varying growth rate is shown in Fig. 3 by solid lines as a function of cavity voltage for various orders. A positive rate indicates potential MP trajectories exist.

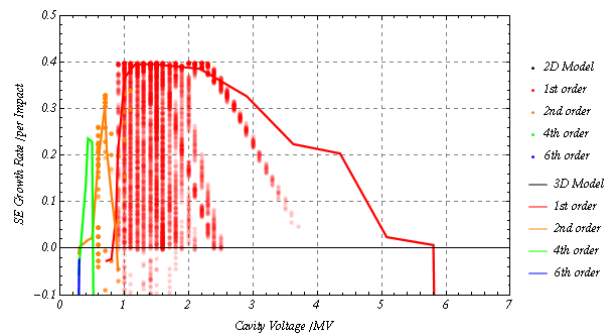


Figure 3: The comparison secondary electron growth rate diagram for the 3D CST simulation results (solid lines) and the 2D simplified single particle tracking model results (dots).

Some common features of MP in the single spoke resonators can be summarized: 1. Single spoke resonators have MP barriers in a wide range of field levels. (Fig. 3) 2. Higher order MP barriers exist at lower field levels, while lower order ones are at higher field levels. (Fig. 3) 3. Lower order MP has wider barriers. (Fig. 3) 4. 1st order MP locates at the spoke roots, while higher order ones locate at the joints of the end shells and the body cylinder.

Copyright © 2015 CC-BY-3.0 and by the respective authors

<sup>#</sup>zyyao@triumf.ca

(Fig. 2) 5. All potential MP locations are at minimum electric field zones that can be described as an RF potential well [17] (Fig. 1 and 2).

## PHENOMENOLOGICAL STUDY

The 3D simulation code can predict the MP well. However the complicated secondary electron trajectories and the intricate field distribution in 3D models hinder the insight into the essence of MP. As the MP has obvious characteristic locations, and is well separated for 1st order and higher order conditions a simplified 2D model with local EM field information is proposed to study the detailed behaviors for each case. One example of 1st order MP is shown in Fig. 4.

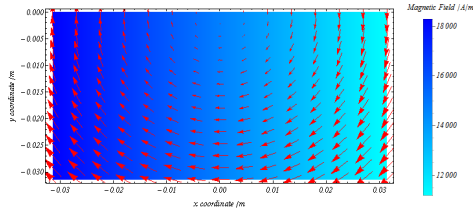


Figure 4: The simplified 2D EM field model for single particle tracking of 1st order MP.

The comparison result of the simplified 2D tracking code and CST 3D simulation is shown in Fig.3. The SEY coefficient of niobium after a 300°C bakeout [18] is used for both codes. The 2D MP model can provide reasonable results. It simplifies the physics image of MP in a complicated 3D structure and so provides a possibility to study the detailed behaviors and understand the fundamental conditions of MP while pointing to an optimization path.

### 2nd Order MP

The secondary electrons impact cavity inner surface in one RF period for 2nd order MP. Higher order MPs have similar behaviors in integer RF period. The electric field pulls out electrons, and accelerates or decelerates them, while the magnetic field bends the trajectories. Therefore the accumulated energy through the interaction with the electric field will be integrated to the impact energy. The peak kinetic energy in one impact period is defined as  $\mathcal{E}_1$ , and the impact energy of the same period is  $\mathcal{E}_2$ . 2D simulation results show proportional relations of  $\mathcal{E}_1$  and  $\mathcal{E}_2/\mathcal{E}_1$  to RF field.

$$\mathcal{E}_1 \propto E^2$$

and

$$\mathcal{E}_2/\mathcal{E}_1 \propto H^2$$

where  $E$  is the electric field and  $H$  is the magnetic field. The impact energy

$$\begin{aligned} \mathcal{E}_{impact} = \mathcal{E}_2 &= \mathcal{E}_1 \frac{\mathcal{E}_2}{\mathcal{E}_1} \propto E^2 H^2 \\ &= \left[ \left( \frac{E_{local}}{E_{acc}} \right)^2 \left( \frac{H_{local}}{E_{acc}} \right)^2 \right] E_{acc}^4 \end{aligned}$$

where  $E_{local}/E_{acc}$  is the local electric field ratio,  $H_{local}/E_{acc}$  is the local magnetic field ratio, and  $E_{acc}$  is the

accelerating gradient. A geometry coefficient of MP is defined in terms of local surface field ratios as

$$k_{MP} = \left[ \left( \frac{E_{local}}{E_{acc}} \right) \left( \frac{H_{local}}{E_{acc}} \right) \right]$$

And the impact energy is simplified

$$\mathcal{E}_{impact} \propto k_{MP}^2 E_{acc}^4$$

The local field ratios are geometry dependent parameters. For certain impact energy, a higher  $k_{MP}$  coefficient satisfies the MP condition at lower accelerating gradients since

$$E_{acc} \propto \sqrt{1/k_{MP}}$$

Also a higher coefficient narrows the bandwidth, which is defined as the width of the MP barrier in the SE growth rate plot, for MP trajectories since

$$BW_E \propto \sqrt{1/k_{MP}}$$

Due to the phase relation of the EM fields in the spoke resonator the magnetic field always bends the electron in one direction towards the spoke root and consequently to a higher magnetic field zone. The stability of MP is dependent on the secondary electron immigration rate, which is considered as impact step in one resonance cycle. It is demonstrated by 2D simulation as

$$\Delta x \propto v_x \propto EH$$

and

$$\Delta x \propto \left[ \left( \frac{E_{local}}{E_{acc}} \right) \left( \frac{H_{local}}{E_{acc}} \right) \right] E_{acc}^2 = k_{MP} E_{acc}^2$$

The impact step length is a geometry dependent parameter. For the same accelerating gradient a higher  $k_{MP}$  coefficient provides a higher drift velocity and pushes the MP to an unstable region. The relationship is consistent with the impact energy limit.

$$E_{acc} \propto \sqrt{1/k_{MP}}$$

and

$$BW_E \propto \sqrt{1/k_{MP}}$$

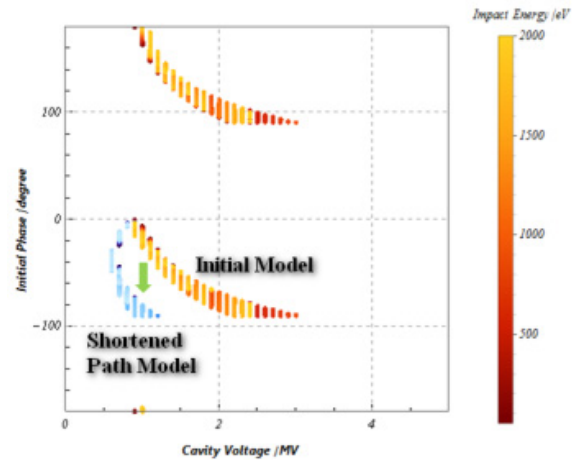


Figure 5: The comparison phase diagram with the shortened geometry path length model.

### 1st Order MP

The 1st order MP is secondary electron resonance in half RF period, which is studied by simulation result diagrams. In the phase diagram, shown with warm color

in Fig. 5, the left and right boundaries are defined the upper and lower phase limits. The electron trajectory to the left of the upper phase limit impacts in more than half an RF period. The electron is considered as a ‘slower’ particle. Thus, shorter geometry path length of resonance can compensate time of flight.

The schematic in Fig. 6 shows the rounding at the spoke root changes the geometry path length. Smaller rounding radius decreases the path length. The comparing result of phase diagram is shown in Fig. 5. The field level of stable electron resonance is moved to left, and the bandwidth is narrowed as inference.

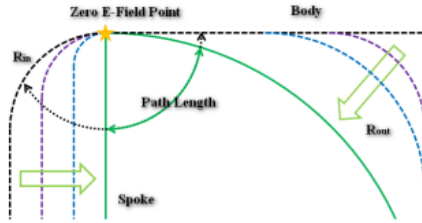


Figure 6: Schematic of varying the geometry path length of resonance electron trajectory. A cross section of high magnetic field region is plotted. The left side stands for spoke, while the right as end wall of resonator.

The impact position diagram is shown in Fig. 7. The top left boundary in negative ordinate area is the minimum impact energy limit when SEY>1, and the bottom right is the maximum energy limit. Thus the lower and higher energy limits of electron resonance are defined.

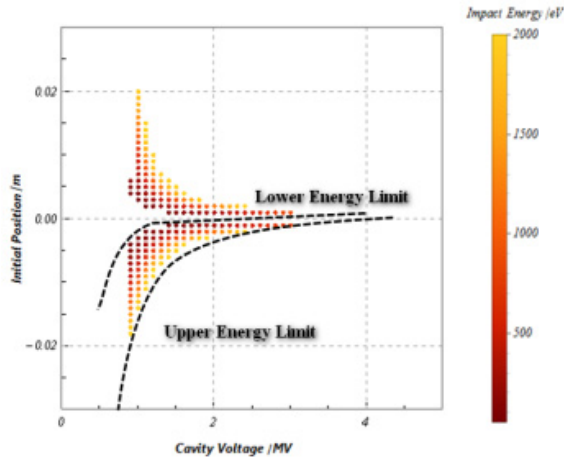


Figure 7: The position diagram of the initial model.

The relation of impact energy and EM field is discussed by the upper and lower equal energy contours. As the electron is only driven by Lorentz force, the impact energy can be assumed as

$$\mathcal{E}_{impact} \propto E^a H^b$$

The electric field along the surface in the model is defined by

$$\frac{E_{local}}{E_{acc}} \propto x$$

Where  $x$  is distance from secondary electron emission position to zero E field point. The magnetic field in the simulation domain is approximate uniform as

$$\frac{H_{local}}{E_{acc}} = constant$$

As the equal energy contour in the position diagram is considered, the impact energy is constant.

$$\mathcal{E}_{impact} \propto E^a H^b = \left[ \left( \frac{E_{local}}{E_{acc}} \right)^2 E_{acc}^2 \right]^a \left[ \left( \frac{H_{local}}{E_{acc}} \right)^2 E_{acc}^2 \right]^b = constant$$

Substituting the constant local magnetic field ratio into the impact energy, it is obtained

$$E_{acc}^{a+b} \propto \left( \frac{E_{local}}{E_{acc}} \right)^{-a}$$

Changing the variables to the cavity voltage and initial position in the position diagram produces

$$V_0^{a+b} \propto x^{-a}$$

or

$$x \propto \frac{1}{V_0^{1+b/a}}$$

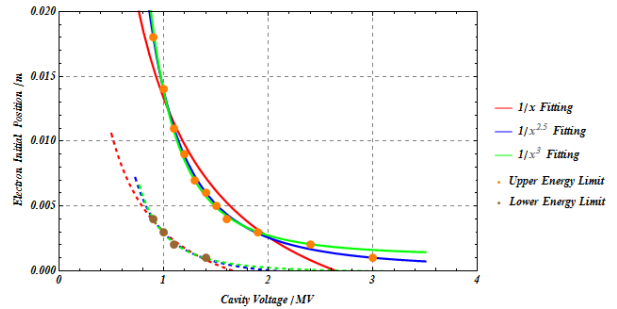


Figure 8: The analytic approximation of the upper (solid line with orange points) and lower (dotted line and brown points) equal energy contour in position diagram. The same fitting formula is plotted in the same color.

The fits of the upper and lower equal energy contour are shown in Fig. 8. The parameter  $b/a$  is fitted in the range of 1.5 to 2. The impact energy is more sensitive to the magnitude of the magnetic field. The higher local magnetic field moves the MP barrier to a lower field level.

### BALLOON VARIANT

The phenomenological discussion shows that geometry optimization can help to suppress the MP in a single spoke cavity. Increasing rounding radius at joints of the end shells and the body cylinder (outer rounding) enhances local RF power density and  $k_{MP}$  for higher order MP, while decreasing rounding radius at spoke roots (inner rounding) increases magnitude of local magnetic field where 1st order MP exists, and reduces resonance path length. Both these geometry trends have suppression effect for MP. Combining maximum outer and minimum inner rounding radius, the resonator geometry is a big balloon. The surface electric and magnetic field distributions are shown in Fig. 9. The minimum electric field zone is right on the spoke root where the magnetic field is higher and more uniform. The geometric acute

angle at the spoke root shortens the phase length of electron resonance. MP barriers are pushed to lower field values and narrowed. The comparison results are shown in the bottom diagram of Fig. 9. The MP suppression effect of the balloon geometry is clearly demonstrated.

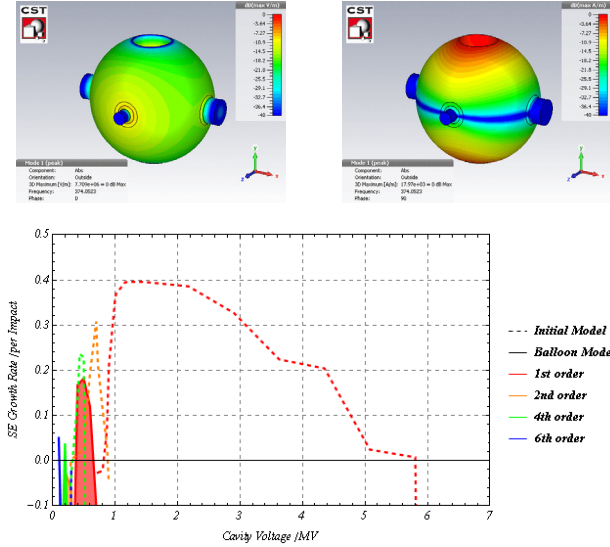


Figure 9: The surface electric and magnetic field distributions of balloon variant (top). The comparison of secondary electron growth rates of the balloon model and the initial model (bottom).

A 325MHz  $\beta=0.3$  single spoke resonator was optimized based on the balloon concept under collaboration between TRIUMF and IBS, shown in Fig. 10. The RF parameters are listed in Table 1, which are comparable with recently designed spoke cavities in a similar  $\beta$  range [5, 10-12]. But the primary advantage of the balloon cavity is the narrow and low level MP barriers, shown in Fig. 11, compared to other designs [7-8, 19-20]. The better mechanical properties are the other superiority. The balloon shape makes the structure rigid, thus it requires less stiffeners to achieve an acceptable mechanical requirement. The helium pressure sensitivity of the unjacketed resonator design is 14Hz/mbar compared to 20Hz/mbar up to 100Hz/mbar for a more typical variant [10-11, 14, 21-22]. The mechanical parameters of jacketed cavity are listed in Table 2.

Table 1: The RF Parameters of the 325MHz  $\beta=0.3$  Balloon Spoke Resonator

Parameters	Value	Units
Frequency	325	MHz
$\beta_g$	0.3	1
$L_{eff} = \beta\lambda$	0.277	m
$E_p/E_{acc}$	3.8	1
$B_p/E_{acc}$	6.1	mT/(MV/m)
R/Q	233	$\Omega$
G	93	$\Omega$

Table 2: The Mechanical Parameters of the Jacketed 325MHz  $\beta=0.3$  Balloon Spoke Resonator

Parameters	Beam Tube	Value	Units
Stress @ 1bar	Fixed	35.9	Mpa
	Free	36.1	
df/dp	Fixed	-9.5	Hz/mbar
	Free	1.6	
LFD	Fixed	-1.9	Hz/(MV/m) <sup>2</sup>
	Free	-10.9	
Tuning	N/A	444	kHz/mm
	N/A	18.2	
	N/A	129.8	

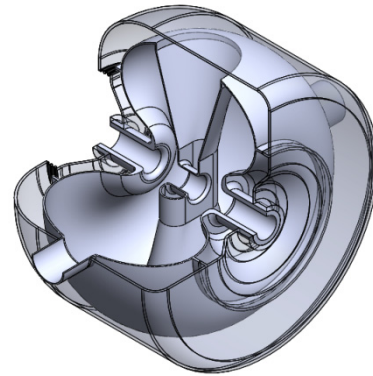


Figure 10: The mechanical model of an optimized 325MHz  $\beta=0.3$  balloon spoke resonator.

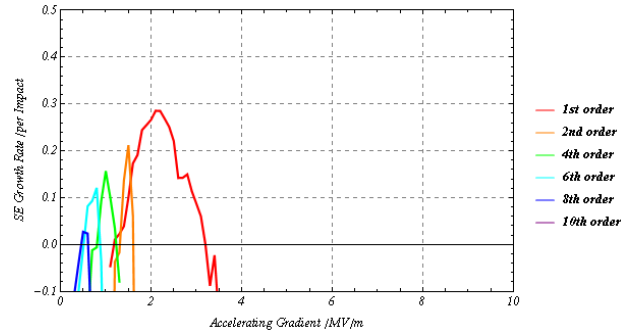


Figure 11: The CST MP simulation result of an optimized 325MHz  $\beta=0.3$  balloon spoke resonator.

## CONCLUSION

A generic MP study is presented in this paper. The characteristic locations for various orders of MP are delineated. A 2D single particle tracking code is utilized to determine the fundamental relation of secondary electron resonance, local EM fields and the resonator geometry.

A phenomenological theory of MP is proposed based on the resonance conditions of the impact energy, phase, and position. It demonstrates that MP in a spoke resonator is observably dependent on the geometry. The MP geometry coefficient ( $k_{MP}$ ) dominates 2nd and higher order electron resonance. 1st order MP is dependent on

several factors such as the magnitude and the uniformity of the local magnetic field. In addition the phase length of the resonance trajectory is a primary parameter to suppress 1st order MP, which is also a variable of the local geometry.

The conception of the balloon variant of a single spoke resonator is presented by the inference of theory and the 3D geometry optimization simulation. It effectively suppresses the MP by moving barriers to lower field levels and narrowing them. An optimized 325MHz  $\beta=0.3$  balloon spoke resonator is proposed under collaboration between TRIUMF and RISP. The balloon variant exhibits a way to overcome the current MP issues of spoke resonators.

## REFERENCES

- [1] P. Derwent, S. Holmes, and V. Lebedev, in Proceedings of the 27th Linear Accelerator Conference, edited by C. Carli (CERN, Geneva, Switzerland, 2014), pp.807-810.
- [2] M. Eshraqi et al., in Proceedings of the 5th International Particle Accelerator Conference, edited by P. Michel (HZDR, Dresden, Germany, 2014), pp.3320-3322.
- [3] D. Vandeplassche et al., in Proceedings of the 5th International Particle Accelerator Conference, edited by P. Michel (HZDR, Dresden, Germany, 2014), pp.3122-3124.
- [4] Z. Li et al., Phys. Rev. ST Accel. Beams 16, 080101 (2013).
- [5] D. O. Jeon and H. J. Kim, in Proceedings of the 27th Linear Accelerator Conference, edited by C. Carli (CERN, Geneva, Switzerland, 2014), pp.775-779.
- [6] M. Sawamura et al., in Proceedings of the 5th International Particle Accelerator Conference, edited by P. Michel (HZDR, Dresden, Germany, 2014), pp.1946-1948.
- [7] C. S. Hopper and J. R. Delayen, Phys. Rev. ST Accel. Beams 16, 102001 (2013).
- [8] T. Kubo et al., in Proceedings of the 27th Linear Accelerator Conference, edited by C. Carli (CERN, Geneva, Switzerland, 2014), pp.1030-1033.
- [9] L. Lu et al., in Proceedings of the 16th International Conference on RF Superconductivity, edited by C. Antoine (CEA-Saclay and IPNO, Paris, France, 2013), pp.988-990.
- [10] L. Ristori et al., in Proceedings of the 16th International Conference on RF Superconductivity, edited by C. Antoine (CEA-Saclay and IPNO, Paris, France, 2013), pp.1187-1192.
- [11] P. Duchesne et al., in Proceedings of the 16th International Conference on RF Superconductivity, edited by C. Antoine (CEA-Saclay and IPNO, Paris, France, 2013), pp.1212-1217.
- [12] Y. He et al., in Proceedings of the 16th International Conference on RF Superconductivity, edited by C. Antoine (CEA-Saclay and IPNO, Paris, France, 2013), pp.868-872.
- [13] T. Khabiboulline et al., in Proceedings of the 3rd International Particle Accelerator Conference, edited by J. Corbett (Louisiana State University, New Orleans, US, 2012), pp.2330-2332.
- [14] C. S. Hopper, H. K. Park, and J. R. Delayen, in Proceedings of the 27th Linear Accelerator Conference, edited by C. Carli (CERN, Geneva, Switzerland, 2014), pp.677-679.
- [15] A. Sukhanov et al., in Proceedings of the 16th International Conference on RF Superconductivity, edited by C. Antoine (CEA-Saclay and IPNO, Paris, France, 2013), pp.112-116.
- [16] CST Studio 2014, www.cst.com.
- [17] S. Belomestnykh and V. Shemelin, Nucl. Instrum. Methods Phys. Res., Sect. A 595, 293 (2008).
- [18] H. Padamsee et al., RF Superconductivity for Accelerators (John Wiley & Sons, New York, 1998).
- [19] P. Berrutti et al., in Proceedings of the North American Particle Accelerator Conference, edited by T. Satogata (LBNL, Pasadena, US, 2013), pp.838-840.
- [20] Z.Q. Li et al., in Proceedings of the 16th International Conference on RF Superconductivity, edited by C. Antoine (CEA-Saclay and IPNO, Paris, France, 2013), pp.939-941.
- [21] P. Sha et al., in Proceedings of the 16th International Conference on RF Superconductivity, edited by C. Antoine (CEA-Saclay and IPNO, Paris, France, 2013), pp.959-961.
- [22] H. Li et al., in Proceedings of the 16th International Conference on RF Superconductivity, edited by C. Antoine (CEA-Saclay and IPNO, Paris, France, 2013), pp.942-945.